

Geophysical Research Letters®

RESEARCH LETTER

10.1029/2021GL096428

Key Points:

- Effects of whistler waves on electron distributions have been studied by a combination of electron magnetohydrodynamics and test-particle simulations
- A whistler wave causes distinct flux enhancements of 10s keV electrons at large pitch angles to form electron butterfly distributions
- Nonlinear Landau trapping contributes to the rapid formation of the electron butterfly distributions

Supporting Information:

Supporting Information may be found in the online version of this article.

Correspondence to:

X. Gao and Q. Lu,
gaoxl@mail.ustc.edu.cn;
qmlu@ustc.edu.cn

Citation:

Ke, Y., Gao, X., Lu, Q., Wang, X., Chen, R., Chen, H., & Wang, S. (2022). Deformation of electron distributions due to Landau trapping by the whistler-mode wave. *Geophysical Research Letters*, 49, e2021GL096428. <https://doi.org/10.1029/2021GL096428>

Received 2 OCT 2021

Accepted 20 JAN 2022

Deformation of Electron Distributions Due to Landau Trapping by the Whistler-Mode Wave

Yangguang Ke^{1,2} , Xinliang Gao^{1,2} , Quanming Lu^{1,2} , Xueyi Wang³ , Rui Chen^{1,2} , Huayue Chen^{1,2} , and Shui Wang^{1,2}

¹Department of Geophysics and Planetary Science, CAS Key Laboratory of Geospace Environment, University of Science and Technology of China, Hefei, China, ²CAS Center for Excellence in Comparative Planetology, Hefei, China, ³Physics Department, Auburn University, Auburn, AL, USA

Abstract Whistler-mode waves can modulate the electron distributions through wave-particle interactions in the Earth's inner magnetosphere. In this paper, we have investigated the effects of the whistler waves on the electron distributions by a combination of electron magnetohydrodynamics and test-particle simulations. Our simulations show a parallel whistler wave becomes gradually oblique during its propagation from the magnetic equator to higher latitudes. Such a whistler wave causes distinct flux increases of tens of keV electrons at large pitch angles to form electron butterfly distributions. This whistler wave traps numerous resonant electrons and transports them from lower latitudes to higher latitudes through nonlinear Landau trapping. Meanwhile, these trapped electrons are efficiently accelerated to higher energies contributing to the rapid formation of electron butterfly distributions at higher latitudes. Our study suggests nonlinear Landau trapping is a potential formation mechanism of the electron butterfly distributions observed in the Earth's inner magnetosphere.

Plain Language Summary Wave-particle interactions are known to play an important role in regulating energetic electron distributions in the Earth's inner magnetosphere. In particular, whistler-mode waves can efficiently modulate the electron distributions by cyclotron and Landau resonant interactions. In this paper, we used a 2-D electron magnetohydrodynamics model to simulate a whistler wave in the dipole geomagnetic field. The simulation results indicate a parallel whistler wave becomes gradually oblique during its propagation from the magnetic equator to high latitudes. Furthermore, a test-particle simulation shows that such a whistler wave can trap and accelerate electrons from the lower latitudes to higher latitudes by nonlinear Landau trapping, which leads to the rapid formation of electron butterfly distributions at tens of keV. Previous studies suggested that nonlinear cyclotron trapping can cause electron butterfly distributions at tens of keV observed in the Earth's magnetosphere. Our study provides a new potential formation mechanism of electron butterfly distributions in the Earth's magnetosphere.

1. Introduction

Whistler-mode waves are one of the most common plasma waves in the Earth's inner magnetosphere (Burtis & Helliwell, 1969; Tsurutani & Smith, 1974, 1977; W. Li et al., 2009), which usually regulate the energetic electron distributions by wave-particle interactions. On the other hand, the modified electron distributions can affect wave evolution. To name a few, nonparallel whistler waves can interact with the energetic electrons through Landau resonance to form a plateau in the parallel velocity distribution, which may play a key role in forming the well-known 0.5 f_{ce} (f_{ce} is the equatorial electron gyrofrequency) power gap of whistler-mode chorus waves (Chen et al., 2021; J. Li et al., 2019). This electron distribution is also conducive to the generation and propagation of highly oblique whistler waves (Ma et al., 2017; Mourenas et al., 2015; W. Li et al., 2016). Besides, whistler waves can modify the electron phase space distribution, and the resultant phase space structures such as phase space holes potentially produce nonlinear wave structures, like Langmuir waves, bipolar and unipolar electric fields (An et al., 2019).

Therefore, how whistler waves affect the energetic electron distributions in the Earth's inner magnetosphere has been an important and attractive topic. Previous studies have shown that whistler waves, as well as magnetosonic waves, can cause the gradual formation of electron butterfly distributions on a time scale from hours to days via quasi-linear diffusion processes (Albert et al., 2016; J. Li et al., 2016; Ma et al., 2016; Ni et al., 2018; Xiao et al., 2015). However, Fennell et al. (2014) and Kurita et al. (2018) reported that the discrete whistler wave

packets lead to bursts of electron butterfly distributions at tens of keV within ~ 30 s. Gan et al. (2020) and Saito et al. (2021) suggested nonlinear cyclotron trapping by whistler waves may play a role in accelerating electrons to form the electron butterfly distributions within such a short time, and whistler waves in their simulations are fixed as parallel propagating along the field line. However, whistler waves should become oblique (Breuillard et al., 2012; Lu et al., 2019) after leaving the equatorial source regions (LeDocq et al., 1998; W. Li et al., 2013), which can also efficiently accelerate electrons by nonlinear Landau trapping (Artemyev et al., 2012; Bell, 1986; Y. K. Hsieh and Omura, 2017; Shklyar & Matsumoto, 2009). By a combination of “electron magnetohydrodynamics” (EMHD) and test-particle simulations, we demonstrate nonlinear Landau trapping in a dipole field by a whistler wave can lead to the rapid formation of electron butterfly distributions.

2. Simulation Model

To model the propagation of a whistler wave in the dipole magnetic field, we have developed a 2-D EMHD simulation based on the gcPIC code (Ke et al., 2021; Lu et al., 2019). The wave propagation has been widely modeled by the ray-tracing simulation (Bortnik et al., 2007; Horne, 1989). However, the EMHD model has the advantage of reproducing the wave phase and amplitude variations and the spatial extent of wave packets (Streltsov et al., 2006). In the simulation, the electrons are modeled as a cold fluid and the ions are considered to be immobile. We solve the motion equations of the cold electron fluid:

$$\frac{\partial \mathbf{V}_e}{\partial t} = -(\mathbf{V}_e \cdot \nabla) \mathbf{V}_e + \frac{q_e}{m_e} (\mathbf{E} + \mathbf{V}_e \times \mathbf{B}), \quad (1)$$

$$\frac{\partial n_e}{\partial t} = -\nabla \cdot (n_e \mathbf{V}_e), \quad (2)$$

$$\mathbf{J} = q_e n_e \mathbf{V}_e, \quad (3)$$

where q_e and m_e are the charge and the rest mass of an electron, n_e and \mathbf{V}_e are the number density and the bulk velocity of the electrons, and \mathbf{J} is the current density. The magnetic fields \mathbf{B} and the electric fields \mathbf{E} are updated by solving Maxwell equations:

$$\frac{\partial \mathbf{E}}{\partial t} = \frac{1}{\mu_0 \epsilon_0} \nabla \times \mathbf{B} - \frac{1}{\epsilon_0} \mathbf{J}, \quad (4)$$

$$\frac{\partial \mathbf{B}}{\partial t} = -\nabla \times \mathbf{E} \quad (5)$$

where μ_0 and ϵ_0 are the permeability and the permittivity of vacuum, respectively. The 2-D EMHD model allows three-dimensional electromagnetic fields and velocities but only 2-D spatial variations in a magnetic meridian plane. A dipole magnetic field is used as the background magnetic field \mathbf{B}_0 . And \mathbf{B}_{0eq} represents the background magnetic field at the equator.

Plasma parameters in the simulation system are set up according to the typical values in the Earth's inner magnetosphere. The simulation domain is in the range of $L = 5.925\text{--}6.075$ and $\lambda \sim -17^\circ\text{--}17^\circ$ (L is the equatorial radial distance of the geomagnetic field in units of Earth Radius R_E and λ is the magnetic latitude). The initial electron number density is uniform $n_e = 5 \text{ cm}^{-3}$. The central point of the simulation domain locates at $L = 6$ and $\lambda = 0^\circ$ where the background magnetic field $B_{0eq,m}$ is about 144 nT and the ratio of electron plasma frequency ω_{pe} to gyrofrequency Ω_{e0} is $\omega_{pe}/\Omega_{e0} \approx 5$. We inject a parallel whistler wave packet at a constant frequency $\omega/\Omega_{e0} = 0.4$ from the magnetic equator with a typical transverse spatial scale about 600 km ($L = 5.94375\text{--}6.0375$) (Agapitov et al., 2017) during time $\Omega_{e0}t = 0\text{--}20,000$ corresponding to ~ 0.8 s. The wave amplitude $B_w/B_{0eq,m}$ increases evenly from 0 to 0.005 during $\Omega_{e0}t = 0\text{--}100$, and remains constant during $\Omega_{e0}t = 100\text{--}20,000$. This whistler wave propagates toward both northward and southward.

A test-particle simulation is used to study the effects of this whistler wave on the energetic electron distributions. We set the energetic electrons subject to a bi-Maxwellian distribution:

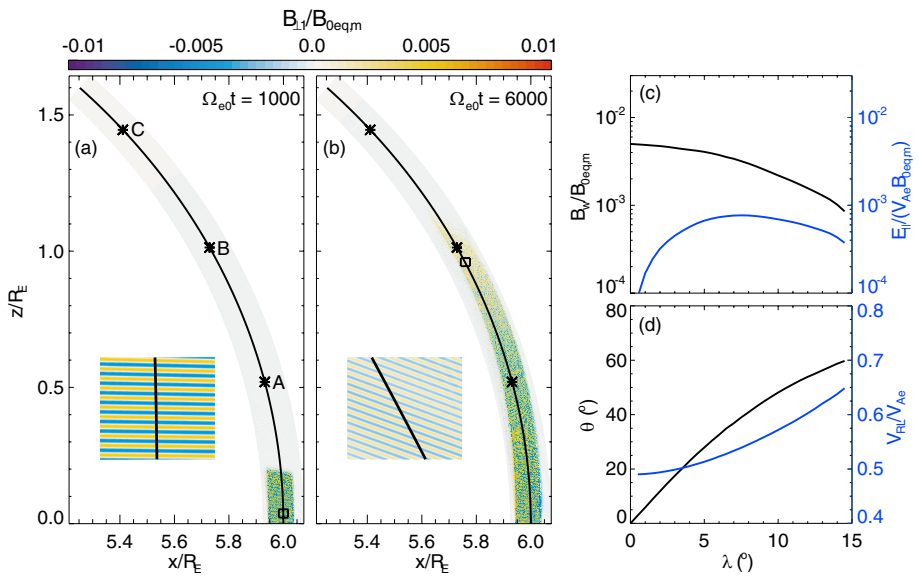


Figure 1. (a and b) The spatial profiles of perpendicular (to the simulation plane) magnetic fluctuations $B_{\perp}/B_{0eq,m}$ in the Cartesian coordinates (x, z) at $\Omega_{e0}t = 1,200$ and $6,000$. Three asterisks marked by “A”, “B”, and “C” are respectively at the magnetic latitudes $\lambda = 5^\circ, 10^\circ$, and 15° on the field line $L = 6$ (black solid line). The enlarged view of the rectangular region is shown at the bottom left of the panel. (c) The time-averaged amplitudes of the magnetic field (black line) and the parallel electric field (blue line) of this wave packet at different latitudes along the field line $L = 6$. (d) The corresponding wave normal angle θ (black line) and Landau resonant velocity V_{RL} (blue line).

$$f(v_{||}, v_{\perp}) = \frac{1}{(2\pi)^{2/3} v_{th||} v_{th\perp}^2 / \zeta} \exp\left(-\frac{v_{||}^2}{2v_{th||}^2} - \frac{v_{\perp}^2}{2v_{th\perp}^2 / \zeta}\right), \quad (6)$$

where $\zeta = 1 + (T_{h\perp}/T_{h||} - 1)(1 - B_{0eq}/B_0)$. $v_{th||}$ ($v_{th\perp}$) is the parallel (perpendicular) thermal velocity and $T_{h||}$ ($T_{h\perp}$) is the parallel (perpendicular) temperature at the magnetic equator. The parallel temperature is $T_{h||} \approx 2.58$ keV and the temperature anisotropy is $T_{h\perp}/T_{h||} = 1.5$. The number density of the energetic electrons is

$$n_h = n_{heq}/\zeta, \quad (7)$$

where n_{heq} is the number density at the magnetic equator. The energetic electron distributions satisfy Liouville's theorem (Lu et al., 2019; Summers et al., 2012). Initially, test particles are placed in the simulation domain within $L = 5.998125$ – 6.001875 , which are distributed in each simulation grid with the particle number proportional to the product of the grid size and n_h . Their positions are random in each grid and their velocities are subject to $f(v_{||}, v_{\perp})$. The total number of test particles is about 114 million. The simulation grid numbers are $N_{||} = 16000$ along the field lines and $N_{\perp} = 400$ along the curves orthogonal to the field lines. The simulation time step is $\Omega_{e0}\Delta t = 0.1$. The boundary conditions are absorbing boundary conditions for waves and reflecting boundary conditions for particles (Lu et al., 2019).

3. Simulation Results

Figure 1 displays the propagation characteristics of the whistler wave packet emitting from the magnetic equator in the simulation. The spatial profiles of the perpendicular (to the simulation plane) magnetic fluctuations $B_{\perp}/B_{0eq,m}$ in the Cartesian coordinates (x, z) at $\Omega_{e0}t = 1,000$ and $6,000$ are shown in Figures 1a and 1b, respectively. Three asterisks marked by “A”, “B”, and “C” locate at the magnetic latitudes $\lambda = 5^\circ, 10^\circ$, and 15° on the field line $L = 6$ (black solid line). The whistler wave fronts reach $\lambda \sim 2^\circ$ at $\Omega_{e0}t = 1,000$ and propagate to the regions around $\lambda = 10^\circ$ at $\Omega_{e0}t = 6,000$. The rectangular areas in Figures 1a and 1b are zoomed in, which indicate that the wave packet remains quasi-parallel near the equator but becomes oblique at $\lambda \sim 10^\circ$. Figure 1c displays the time-averaged amplitudes of the magnetic field (black line) and the parallel electric field (blue line) of this wave packet at different latitudes along the field line $L = 6$. When the wave packet propagates from the equator

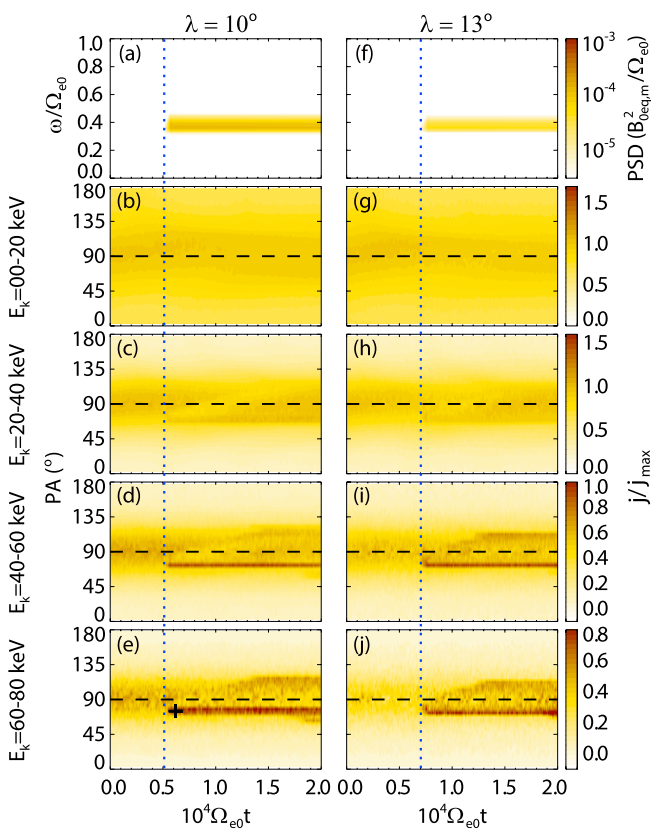


Figure 2. (a and f) The power spectral density of the wave magnetic field at the magnetic latitudes $\lambda = 10^\circ$ and 13° on the field line $L = 6$. (b–e and g–j) The time evolutions of electron pitch angle (PA) distributions j/j_{\max} at different energy channels from $E_k = 0\text{--}20 \text{ keV}$ to $E_k = 60\text{--}80 \text{ keV}$ at $\lambda = 10^\circ$ and 13° , respectively. And j_{\max} is the maximum value of the local electron differential flux j . The plus symbol indicates a zone ($\Omega_{e0}t = 6,000$, PA = $75^\circ\text{--}80^\circ$).

and the blue line represents the distribution at $\Omega_{e0}t = 6,000$. The Landau resonant velocity V_{RL} marked by the vertical dotted line is $0.57V_{Ae}$ at $\lambda = 10^\circ$. In the parallel velocity distribution, a beam-like electron population forms at $\lambda = 10^\circ$ around the Landau resonant velocity when the wave packet passes.

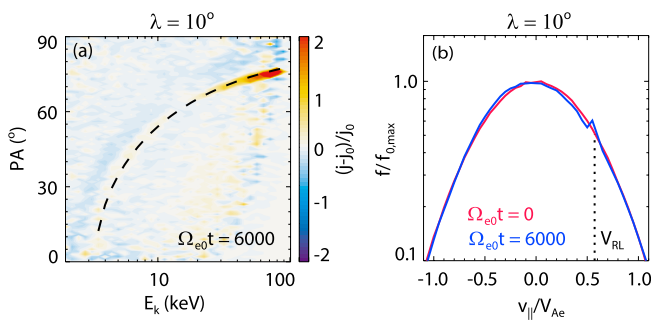


Figure 3. (a) The electron flux variation $(j - j_0)/j_0$ in the pitch angle-energy space at $\lambda = 10^\circ$ on the field line $L = 6$ at $\Omega_{e0}t = 6,000$, where j_0 is the initial value of j . The black dashed line marks the Landau resonant energies at different pitch angles. (b) The parallel velocity distributions of electrons at $\lambda = 10^\circ$ on the field line $L = 6$. The vertical dotted line denotes the Landau resonant velocity.

to $\lambda \sim 15^\circ$, its magnetic field decays gradually while its parallel electric field first enhances and then decays slowly. Meanwhile, the wave normal angle θ increases gradually from 0° to $\sim 60^\circ$ and the Landau resonant velocity V_{RL} increases gradually from $0.49 V_{Ae}$ to $0.65 V_{Ae}$, where $V_{Ae} = B_{0eq,m}/\sqrt{\mu_0 m_e n_e}$ is the electron Alfvén velocity (Figure 1d). Besides, Figures 1a and 1b show that the wave packet gradually propagates to larger L-shells, but the test particles are still inside the wave fields in the simulation.

Figure 2 demonstrates the effects of the whistler wave on the electron pitch angle distributions at higher latitudes. Figures 2a and 2f exhibit the power spectral density (PSD) of the wave magnetic field at $\lambda = 10^\circ$ and $\lambda = 13^\circ$ on the field line $L = 6$. Figures 2b–2e and 2g–2j present the time evolutions of the electron pitch angle (PA) distributions at different energy channels at $\lambda = 10^\circ$ and $\lambda = 13^\circ$, respectively. The electron fluxes j/j_{\max} (j_{\max} is the maximum value of the local electron differential flux j) change slightly at the energy channel $E_k = 0\text{--}20 \text{ keV}$ (Figures 2b and 2g). But significant electron flux increases at PA $\approx 65^\circ\text{--}80^\circ$ appear immediately at the energy channels above 20 keV after the arrival of the wave and exist during the passing time of the whistler wave (Figures 2c–2e and 2h–2j). Besides, the electron flux increases are more remarkable at larger energy channels. Interestingly, the other flux increases at PA $\approx 100^\circ\text{--}120^\circ$ occur after a period at the energy channels $E_k = 40\text{--}60 \text{ keV}$ and $E_k = 60\text{--}80 \text{ keV}$. Consequently, these flux increases near 90° PA caused by the whistler wave lead to the electron butterfly distributions.

Figure 3a shows the electron flux variation $(j - j_0)/j_0$ in the pitch angle-energy space at $\lambda = 10^\circ$ on the field line $L = 6$ at $\Omega_{e0}t = 6,000$, where j_0 is the initial value of j . The black dashed line marks the Landau resonant energies at different pitch angles (named as Landau resonant line). The electron fluxes decrease in the left regions near the Landau resonant line but increase around the Landau resonant line. The significant electron flux enhancements take place around the Landau resonant line at $E_k > 20 \text{ keV}$. It reveals that the electron flux increases at tens of keV near 90° PA are due to Landau resonant interactions. Figure 3b exhibits the parallel velocity distributions of the energetic electrons at $\lambda = 10^\circ$. The red line represents the distribution at $\Omega_{e0}t = 0$ and the blue line represents the distribution at $\Omega_{e0}t = 6,000$. The Landau resonant velocity V_{RL} marked by the vertical dotted line is $0.57V_{Ae}$ at $\lambda = 10^\circ$. In the parallel velocity distribution, a beam-like electron population forms at $\lambda = 10^\circ$ around the Landau resonant velocity when the wave packet passes.

We traced the motions of these electrons in the zone ($\Omega_{e0}t = 6,000$, PA = $75^\circ\text{--}80^\circ$, and $E_k = 60\text{--}80 \text{ keV}$) marked by a plus symbol in Figure 2e, and found that these electrons can be classified into two groups: trapped electrons and transient resonant electrons. Their trajectories are plotted in Figure S1 in Supporting Information S1. The proportion of these trapped electrons is up to 68%. The electron flux variation in this zone is $(j - j_0)/j_0 \sim 2.0$ (seen in Figure 3a), which gives $(j - j_0)/j \sim 67\%$. It indicates that these trapped electrons contribute to the significant electron flux increases at tens of keV at PA $\approx 65^\circ\text{--}80^\circ$. By the same method of particle tracking, we found the electron flux increases at tens of keV at PA $\approx 100^\circ\text{--}120^\circ$ also result from these trapped electrons that have been reflected due to the magnetic mirror effect. Therefore, nonlinear Landau trapping leads to the rapid formation of the electron butterfly distributions.

Figures 4a–4c show the time, the parallel velocity, and the kinetic energy as functions of the magnetic latitude λ for a transient resonant electron (black solid lines) and a trapped electron (blue lines). This transient resonant electron

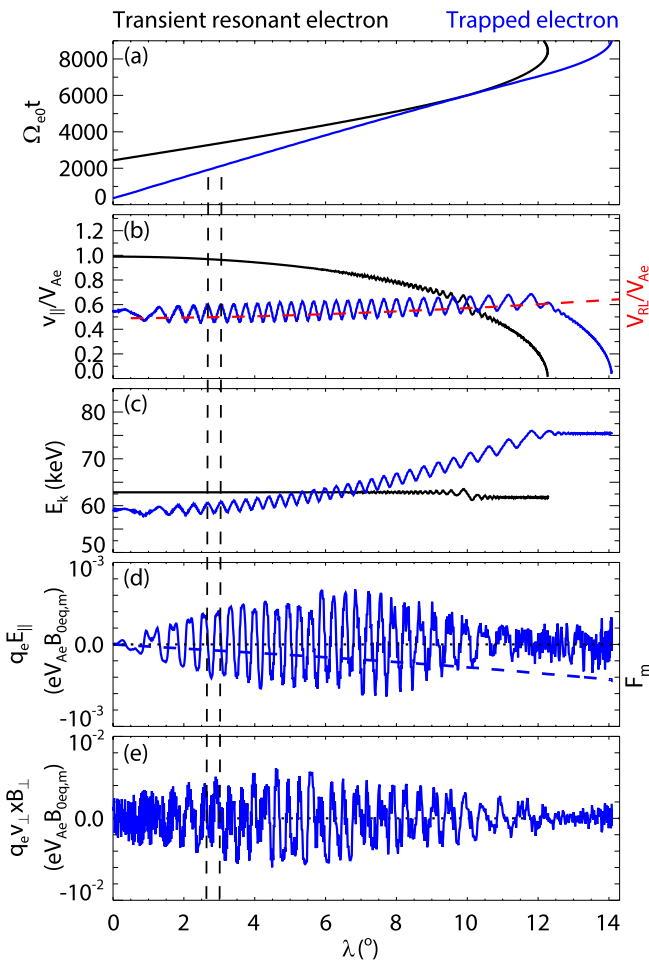


Figure 4. The (a) time, (b) parallel velocity $v_{||}$ and (c) kinetic energy E_k as functions of magnetic latitude λ for a transient resonant electron (black solid lines) and a trapped electron (blue lines). The Landau resonant velocity V_{RL} is indicated by the red dashed line. (d) The parallel electric field force of the wave $q_e E_{||}$ (blue line) and the magnetic mirror force of the background magnetic field F_m (blue dashed line) on this trapped electron. (e) The parallel magnetic force of the wave $q_e v_{\perp} \times B_{\perp}$ (blue line) smoothed by moving average method on this trapped electron.

resonates with the wave packet via Landau resonance at $\lambda \sim 10^\circ$ in a short time, whose energy remains nearly constant (Figures 4a–4c). This trapped electron is trapped by the wave packet in Landau resonance from $\lambda \sim 1^\circ$ to $\lambda \sim 12^\circ$ during $\Omega_{e0}t \sim 1,000$ –7,000 (about 0.24 s). Meanwhile, its parallel velocity $v_{||}$ fluctuates around the Landau resonant velocity V_{RL} and its energy E_k rises in fluctuation from 60 to 75 keV (Figures 4a–4c). The electron energy is $E_k = m_e c^2 (\gamma - 1)$, where c is the speed of light, $\gamma = 1/\sqrt{1 - v^2/c^2}$ is the Lorentz factor, and v is the electron velocity. The parallel motion of this trapped electron is controlled by the parallel electromagnetic force expressed as

$$F_{||} \approx q_e E_{||} + F_m + q_e v_{\perp} \times B_{\perp}, \quad (8)$$

where $F_m = -\mu \nabla_{||} B_0$ is the magnetic mirror force due to the background magnetic field and B_{\perp} is the perpendicular wave magnetic field. Here $\mu = \gamma m_e v_{\perp}^2/(2B_0)$ is the electron magnetic moment. Figure 4d shows that the parallel electric field force $q_e E_{||}$ (blue solid line) fluctuates around zero, while F_m (blue dashed line) is negative whose absolute value increases with the increase of λ . Figure 4e shows that $q_e v_{\perp} \times B_{\perp}$ (blue solid line) smoothed by moving average method fluctuates synchronously with $q_e E_{||}$ but has the amplitude much larger than that of $q_e E_{||}$ during the trapping periods. It suggests that $q_e v_{\perp} \times B_{\perp}$ dominates the trapping process for this electron. Two vertical dashed lines denote two adjacent peaks of $v_{||}$ and E_k , which almost correspond to the zero points of $q_e E_{||}$ and smoothed $q_e v_{\perp} \times B_{\perp}$. The time duration between two lines is a trapping period $T_t \approx 210 \Omega_{e0}^{-1}$, and the trapping frequency is about $0.033 \Omega_{e0}$. The trapping frequency can be also estimated by the theoretical formula (Bell, 1986; Y. K. Hsieh and Omura, 2018)

$$\omega_{tr}^2 = \frac{q_e k_{||}}{m_e} \left[E_{||} J_0 \left(\frac{\gamma k_{\perp} v_{\perp}}{\Omega_e} \right) + v_{\perp} B_R J_{-1} \left(\frac{\gamma k_{\perp} v_{\perp}}{\Omega_e} \right) + v_{\perp} B_L J_1 \left(\frac{\gamma k_{\perp} v_{\perp}}{\Omega_e} \right) \right], \quad (9)$$

where $k_{||}$ (k_{\perp}) is the parallel (perpendicular) wave number and B_R (B_L) is the right-hand (left-hand) circular component of the perpendicular wave magnetic field B_{\perp} given by

$$B_R = \frac{B_{\perp 1} + B_{\perp 2}}{2}, \quad B_L = \frac{B_{\perp 1} - B_{\perp 2}}{2}. \quad (10)$$

Here $B_{\perp 1}$ is the component of B_{\perp} in the simulation plane. The J_n are the Bessel functions of the first kind of order n . The theoretical value of the trapping frequency is estimated as $\omega_{tr} \approx 0.033 \Omega_{e0}$, consistent with the result in the simulation.

We also traced the motions of these electrons in the beam-like distribution at $v_{||}/V_{Ae} = 0.565$ –0.575 at $\Omega_{e0}t = 6,000$ in Figure 3b. The trajectories of these electrons including trapped and untrapped electrons are presented in Figure S2 in Supporting Information S1. The proportion of these trapped electrons is about 60%. Most of these trapped electrons are trapped from the lower latitudes $\lambda < 5^\circ$. The results indicate that Landau trapping leads to the beam-like electron population in the parallel velocity distribution.

4. Conclusions and Discussion

In this paper, we use a 2-D EMHD simulation to model a whistler wave propagating in a dipole magnetic field and study its effects on the energetic electron distributions by a test-particle simulation. Our simulation results demonstrate this whistler wave can significantly modify the energetic electron distributions through nonlinear Landau trapping. The principal conclusions are summarized below.

1. The effects of a whistler wave on the energetic electron distributions have been studied by a combination of EMHD and test-particle simulations, which show that a parallel whistler wave becomes gradually oblique during its propagation from the magnetic equator to higher latitudes.
2. Such a whistler wave causes distinct flux increases of 10s keV electrons at large (near 90°) pitch angles to form electron butterfly distributions at higher latitudes.
3. Nonlinear Landau trapping by this whistler wave leads to the rapid formation of the electron butterfly distributions.

This whistler wave traps numerous electrons by Landau resonance from lower latitudes to higher latitudes and accelerates them to higher energies since the local Landau resonant velocity also increases. These trapped electrons are accelerated significantly to form the electron butterfly distributions. Our study provides a new potential formation mechanism of electron butterfly distributions in the Earth's magnetosphere.

Landau trapping is a nonlinear acceleration process to form the electron butterfly distributions rapidly within ~1s. It is distinct from the quasi-linear diffusion process driven by plasmaspheric hiss due to Landau resonance (Albert et al., 2016), which causes the gradual formation of the butterfly distributions on a time scale from hours to days. Landau trapping is more likely to occur for the intense coherent and narrowband waves such as chorus waves, potentially leading to rapid bursts of electron butterfly distributions that have been observed in the Earth's magnetosphere (Fennell et al., 2014; Kurita et al., 2018).

Previous observations showed that whistler waves could increase field-aligned electron fluxes at lower energies by Landau resonant interactions (J. Li et al., 2019; Wang et al., 2020). In our simulation, the electrons at lower energies are easily trapped by the whistler wave (see Figure S2 in Supporting Information S1). But the electron flux increment $(j - j_0)/j_0$ at lower energies around the Landau resonant line is small (Figure 3a). The potential reason is related to the initial bi-Maxwellian electron distribution. We assume the number density of electrons at energy E_k is f , and αf of electrons at E_k can be trapped and accelerated to $E_k + \Delta E_k$ at which the electron number density is $f + \delta f$. Then $\alpha f/(f + \delta f) = \alpha/(1 + \delta)$ is the contribution of these trapped electrons to the electron flux increment. If α changes slightly, $\alpha/(1 + \delta)$ becomes smaller when δ become larger. Here δ is approximately proportional to the gradient of $f(E_k)$, which is usually larger at lower energies in the bi-Maxwellian distribution.

In this paper, we studied the deformation of electron distributions caused by a whistler wave. However, the modified electron distributions may affect the generation and evolution of whistler waves or other plasma waves, which can be taken into account in future studies.

Data Availability Statement

Simulation datasets for this research are available at the following link <https://doi.org/10.5281/zenodo.5866986>.

Acknowledgments

This work is supported by the National Science Foundation of China (NSFC) grants 42104155, the China Postdoctoral Science Foundation (Grant 2021M693049), and USTC Research Funds of the Double First-Class Initiative (YD3420002001), the Fundamental Research Funds for the Central Universities (WK3420000013, WK2080000150), and "USTC Tang Scholar" program. The simulations were carried out at National Supercomputer Center in Tianjin, and the calculations were performed on TianHe-1 (A).

References

- Agapitov, O., Blum, L. W., Mozer, F. S., Bonnell, J. W., & Wygant, J. (2017). Chorus whistler wave source scales as determined from multipoint Van Allen Probe measurements. *Geophysical Research Letters*, 44(6), 2634–2642. <https://doi.org/10.1002/2017gl072701>
- Albert, J. M., Starks, M. J., Horne, R. B., Meredith, N. P., & Glauert, S. A. (2016). Quasi-linear simulations of inner radiation belt electron pitch angle and energy distributions. *Geophysical Research Letters*, 43(6), 2381–2388. <https://doi.org/10.1002/2016gl067938>
- An, X., Li, J., Bortnik, J., Decyk, V., Kletzing, C., & Hospodarsky, G. (2019). Unified view of nonlinear wave structures associated with whistler-mode chorus. *Physical Review Letters*, 122(4), 045101. <https://doi.org/10.1103/physrevlett.122.045101>
- Artemyev, A. V., Krasnoselskikh, V. V., Agapitov, O. V., Mourenas, D., & Rolland, G. (2012). Non-diffusive resonant acceleration of electrons in the radiation belts. *Physics of Plasmas*, 19(12). <https://doi.org/10.1063/1.4769726>
- Bell, T. F. (1986). The wave magnetic field amplitude threshold for nonlinear trapping of energetic gyroresonant and Landau resonant electrons by nonducted VLF waves in the magnetosphere. *Journal of Geophysical Research*, 91(A4), 4365–4379. <https://doi.org/10.1029/ja091ia04p04365>
- Bortnik, J., Thorne, R. M., & Meredith, N. P. (2007). Modeling the propagation characteristics of chorus using CRRES suprathermal electron fluxes. *Journal of Geophysical Research*, 112(A8). <https://doi.org/10.1029/2006ja012237>
- Breuillard, H., Zaliznyak, Y., Krasnoselskikh, V., Agapitov, O., Artemyev, A., & Rolland, G. (2012). Chorus wave-normal statistics in the Earth's radiation belts from ray tracing technique. *Annales Geophysicae*, 30(8), 1223–1233. <https://doi.org/10.5194/angeo-30-1223-2012>
- Burtis, W. J., & Helliwell, R. A. (1969). Banded chorus-A new type of VLF radiation observed in the magnetosphere by OGO 1 and OGO 3. *Journal of Geophysical Research*, 74(11), 3002–3010. <https://doi.org/10.1029/ja074i011p03002>
- Chen, H., Gao, X., Lu, Q., Sauer, K., Chen, R., Yao, J., & Wang, S. (2021). Gap formation around 0.5 Ωe of whistler-mode waves excited by electron temperature anisotropy. *Journal of Geophysical Research: Space Physics*, 126(2), e2020JA028631. <https://doi.org/10.1029/2020ja028631>
- Fennell, J. F., Roeder, J. L., Kurth, W. S., Henderson, M. G., Larsen, B. A., & Hospodarsky, G. (2014). Van Allen Probes observations of direct wave-particle interactions. *Geophysical Research Letters*, 41(6), 1869–1875. <https://doi.org/10.1002/2013gl059165>

- Gan, L., Li, W., Ma, Q., Artemyev, A. V., & Albert, J. M. (2020). Unraveling the formation mechanism for the bursts of electron butterfly distributions: Test particle and quasilinear simulations. *Geophysical Research Letters*, 47(21). <https://doi.org/10.1029/2020gl090749>
- Horne, R. B. (1989). Path-integrated growth of electrostatic waves: The generation of terrestrial myriametric radiation. *Journal of Geophysical Research*, 94(A7), 8895–8909. <https://doi.org/10.1029/ja094ia07p08895>
- Hsieh, Y. K., & Omura, Y. (2017). Nonlinear dynamics of electrons interacting with oblique whistler mode chorus in the magnetosphere. *Journal of Geophysical Research: Space Physics*, 122(1), 675–694. <https://doi.org/10.1002/2016ja023255>
- Hsieh, Y. K., & Omura, Y. (2018). Nonlinear damping of oblique whistler mode waves via Landau resonance. *Journal of Geophysical Research: Space Physics*, 123(9), 7462–7472. <https://doi.org/10.1029/2018ja025848>
- Ke, Y., Chen, L., Gao, X., Lu, Q., Wang, X., Chen, R., et al. (2021). Whistler-mode waves trapped by density irregularities in the Earth's magnetosphere. *Geophysical Research Letters*, 48(7). <https://doi.org/10.1029/2020gl092305>
- Kurita, S., Miyoshi, Y., Kasahara, S., Yokota, S., Kasahara, Y., Matsuda, S., et al. (2018). Deformation of electron pitch angle distributions caused by upper band chorus observed by the Arase satellite. *Geophysical Research Letters*, 45(16), 7996–8004. <https://doi.org/10.1029/2018gl079104>
- LeDocq, M. J., Gurnett, D. A., & Hospodarsky, G. B. (1998). Chorus source locations from VLF Poynting flux measurements with the Polar spacecraft. *Geophysical Research Letters*, 25(21), 4063–4066. <https://doi.org/10.1029/1998gl900071>
- Li, J., Bortnik, J., An, X., Li, W., Angelopoulos, V., Thorne, R. M., et al. (2019). Origin of two-band chorus in the radiation belt of Earth. *Nature Communications*, 10(1), 4672. <https://doi.org/10.1038/s41467-019-12561-3>
- Li, J., Ma, Q., Bortnik, J., Li, W., An, X., Reeves, G. D., et al. (2019). Parallel acceleration of suprathermal electrons caused by whistler-mode hiss waves. *Geophysical Research Letters*, 46(22), 12675–12684. <https://doi.org/10.1029/2019gl085562>
- Li, J., Ni, B., Ma, Q., Xie, L., Pu, Z., Fu, S., et al. (2016). Formation of energetic electron butterfly distributions by magnetosonic waves via Landau resonance. *Geophysical Research Letters*, 43(7), 3009–3016. <https://doi.org/10.1002/2016gl067853>
- Li, W., Bortnik, J., Thorne, R. M., Cully, C. M., Chen, L., Angelopoulos, V., et al. (2013). Characteristics of the Poynting flux and wave normal vectors of whistler-mode waves observed on THEMIS. *Journal of Geophysical Research: Space Physics*, 118(4), 1461–1471. <https://doi.org/10.1002/jgra.50176>
- Li, W., Mourenas, D., Artemyev, A. V., Bortnik, J., Thorne, R. M., Kletzing, C. A., et al. (2016). Unraveling the excitation mechanisms of highly oblique lower band chorus waves. *Geophysical Research Letters*, 43(17), 8867–8875. <https://doi.org/10.10202/2016gl070386>
- Li, W., Thorne, R. M., Angelopoulos, V., Bortnik, J., Cully, C. M., Ni, B., et al. (2009). Global distribution of whistler-mode chorus waves observed on the THEMIS spacecraft. *Geophysical Research Letters*, 36(9). <https://doi.org/10.1029/2009gl037595>
- Lu, Q., Ke, Y., Wang, X., Liu, K., Gao, X., Chen, L., & Wang, S. (2019). Two-dimensional gcPIC simulation of rising-tone chorus waves in a dipole magnetic field. *Journal of Geophysical Research: Space Physics*, 124(6), 4157–4167. <https://doi.org/10.1029/2019ja026586>
- Ma, Q., Artemyev, A. V., Mourenas, D., Li, W., Thorne, R. M., Kletzing, C. A., et al. (2017). Very oblique whistler mode propagation in the radiation belts: Effects of hot plasma and Landau damping. *Geophysical Research Letters*, 44(24), 12057–12066. <https://doi.org/10.10202/2017gl075892>
- Ma, Q., Li, W., Thorne, R. M., Bortnik, J., Kletzing, C. A., Kurth, W. S., & Hospodarsky, G. B. (2016). Electron scattering by magnetosonic waves in the inner magnetosphere. *Journal of Geophysical Research: Space Physics*, 121(1), 274–285. <https://doi.org/10.1002/2015ja021992>
- Mourenas, D., Artemyev, A. V., Agapitov, O. V., Krasnoselskikh, V., & Mozer, F. S. (2015). Very oblique whistler generation by low-energy electron streams. *Journal of Geophysical Research: Space Physics*, 120(5), 3665–3683. <https://doi.org/10.1002/2015ja021135>
- Ni, B., Zou, Z., Fu, S., Cao, X., Gu, X., & Xiang, Z. (2018). Resonant scattering of radiation belt electrons by off-equatorial magnetosonic waves. *Geophysical Research Letters*, 45(3), 1228–1236. <https://doi.org/10.1002/2017gl075788>
- Saito, S., Kurita, S., Miyoshi, Y., Kasahara, S., Yokota, S., Keika, K., et al. (2021). Data-driven simulation of rapid flux enhancement of energetic electrons with an upper-band whistler burst. *Journal of Geophysical Research: Space Physics*, 126(4). <https://doi.org/10.1029/2020ja028979>
- Shklyar, D. & Matsumoto, H. (2009). Oblique whistler-mode waves in the inhomogeneous magnetospheric plasma: Resonant interactions with energetic charged particles. *Surveys in Geophysics*, 30(2), 55–104. <https://doi.org/10.1007/s10712-009-9061-7>
- Streltsov, A. V., Lampe, M., Manheimer, W., Ganguli, G., & Joyce, G. (2006). Whistler propagation in inhomogeneous plasma. *Journal of Geophysical Research*, 111(A3). <https://doi.org/10.1029/2005ja011357>
- Summers, D., Omura, Y., Miyashita, Y., & Lee, D. H. (2012). Nonlinear spatiotemporal evolution of whistler mode chorus waves in Earth's inner magnetosphere. *Journal of Geophysical Research: Space Physics*, 117(A9). <https://doi.org/10.1029/2012ja017842>
- Tsurutani, B. T., & Smith, E. J. (1974). Postmidnight chorus: A substorm phenomenon. *Journal of Geophysical Research*, 79(1), 118–127. <https://doi.org/10.1029/ja079i001p00118>
- Tsurutani, B. T., & Smith, E. J. (1977). Two types of magnetospheric ELF chorus and their substorm dependences. *Journal of Geophysical Research*, 82(32), 5112–5128. <https://doi.org/10.1029/ja082i032p05112>
- Wang, Z., Su, Z., Liu, N., Dai, G., Zheng, H., Wang, Y., & Wang, S. (2020). Suprathermal electron evolution under the competition between plasmaspheric plume hiss wave heating and collisional cooling. *Geophysical Research Letters*, 47(19). <https://doi.org/10.1029/2020gl089649>
- Xiao, F., Yang, C., Su, Z., Zhou, Q., He, Z., He, Y., et al. (2015). Wave-driven butterfly distribution of Van Allen belt relativistic electrons. *Nature Communications*, 6, 8590. <https://doi.org/10.1038/ncomms9590>